

## Analysis of mixing in a helical microchannel

Pravat Rajbanshi <sup>1</sup> and Animangsu Ghatak<sup>1,2,\*</sup><sup>1</sup>*Department of Chemical Engineering, Indian Institute of Technology Kanpur, Kanpur 208016, India*<sup>2</sup>*Center for Environmental Science and Engineering, Indian Institute of Technology Kanpur, Kanpur 208016, India*

(Received 12 July 2019; accepted 21 May 2020; published 22 June 2020)

Experiments on the mixing of two different fluids at low Reynolds number inside helical channels have shown that their curvature and torsion induce secondary flow at the channel cross section, which enhances mixing between liquids. While these channels are mostly of symmetric cross section, e.g., circular and rectangular, recent experiments suggest that helical channels with asymmetric cross sections can enhance mixing even further. There have, however, been few systematic studies on the coupled effect of the asymmetry of a channel cross section and its three-dimensional orientation on the mixing of fluid streams. In this regard, we have examined mixing between three differently dyed streams of cross-linkable silicone material inside triple-helical microchannels; we have also simulated the flow of liquids through such channels using FLUENT software. Our results show that the length of the interface that separates different liquids at any cross section varies linearly with a nondimensional parameter involving curvature, torsion, axial length, and helix radius of the channel. Moreover, mixing efficiency increases with Péclet number, the exponent of variation being dependent on the Reynolds number of flow.

DOI: [10.1103/PhysRevFluids.5.064502](https://doi.org/10.1103/PhysRevFluids.5.064502)

### I. INTRODUCTION

Mixing between fluid streams at microscale is important in the context of many microfluidic applications, e.g., microfluidic total analytical systems [1,2], biochemical analysis [3] such as DNA sequencing [4] and cell lyses [5], transient analysis of intracellular signal transduction processes [6,7], and several targeted applications [8–10]. Rapid mixing is desired also for many microfluidic devices, e.g., homogenization of solutions of reagents used in chemical reactions [11]; dispersion of materials [12]; generation of water droplets in a continuous flow of oil [13]; and in biology for ultrafast mixing of reactants and enzymes inside glands, e.g., for rapid release of chemicals by certain insects for their defense [14]. The micromixers are of two types: active and passive [8,15]. Active micromixers involve an externally driven agitation device, whereas passive ones make use of specific features of their geometry for the agitation to occur. Examples of passive microfluidic mixers are T-shaped [16,17], Y-shaped [18], and L-shaped [19] channels; a staggered herringbone mixer [8,20]; splitting flow [21]; and a split and recombine mixer [22,23]: in all these mixers mixing essentially occurs by chaotic advection induced by time dependent yet two-dimensional flow. Chaotic advection results in an increase in the interface between two different liquids, which enhances the extent of molecular diffusion and consequent mixing. Chaotic advection occurs also in time invariant yet three-dimensional flow. For example, flow through a planar curved channel results in a secondary circumferential flow in addition to the primary axial flow [24–26]. For a spiral channel, for which helix angle  $\theta = 90^\circ$ , this secondary flow results in two oppositely rotating

\*aghatak@iitk.ac.in

vortices at the channel cross section, known as the Dean vortices. The flow through such channel is characterized by a dimensionless number, the Dean number, defined as  $Dn = (a\kappa)^{0.5} Re$  in which  $Re = \bar{v}d_h\rho/\mu$ , where  $\bar{v}$  is the average velocity of flow,  $d_h$  is the hydraulic diameter of the channel,  $\mu$  is the viscosity of the liquid,  $\kappa$  defines the curvature of the channel axis, and  $a$  defines the helix radius. At small  $Dn$  number, the centrifugal force is not sufficient to split the axial flow in the channel, but when the  $Dn$  number gets large enough, the axial flow inside the tube is perturbed by a secondary flow in the transverse plane, which can induce chaotic advection in the laminar regime [27–29]. Apart from the spiral channel, fluid flow has been examined also for a helical channel [28,29], the geometry of which is defined also by the torsion of the channel axis in addition to its curvature, defined as  $\tau = \sin\theta \cos\theta/a$  and  $\kappa = \sin^2\theta/a$ , respectively [30,31]. Both these geometric parameters have been shown to affect the strength of this secondary flow and the number of vortices [28–30]. It has been shown also [26,32] that such secondary flow enhances mixing between liquids over that which occurs in straight channels. While the cross sections of all these channels remain circular, asymmetry in a channel cross section is expected to bring in additional complexity, which has not been examined in sufficient detail [33–38]. For example, flow through helical channels with square, triangle, and elliptic cross sections has been examined in the context of enhancement of heat transfer area [33], and air-water two-phase flow [34–36]. However, not much work has been done to characterize mixing and particularly evolution of the mixing interface between fluid streams [37,38]. However, the combined effect of an asymmetric cross section and the three-dimensional orientation of the channels has not been examined to any detail in the literature.

In order to understand the coupled effect of channel geometry and Reynolds number of flow on the extent of mixing between different liquids, and on the evolution of the interface between them, we performed both experiments and flow simulations. We used triple-helical microchannels embedded monolithically inside a poly(dimethylsiloxane) (PDMS) block, inside which we pumped three streams of differently dyed cross-linkable silicone [room temperature vulcanizing (RTV)] material. The RTV was cross-linked and the cross-linked mold was subsequently recovered. Analysis of images of the cross section of the mold at different axial lengths showed the extent of mixing between different streams. In order to obtain more detailed qualitative information about evolution of the interface between different liquid streams, three-dimensional (3D) simulations of species transport were performed using commercially available FLUENT software. These analyses show that contour length of the interface between different streams varies linearly with the axial length of the channel but exhibits nonlinear dependence on the helix angle. At low Reynolds number, a strong secondary flow field can occur in these channels because of the occurrence of multiple vortices in the constituent lobe, thereby enhancing the extent of mixing.

## II. MATERIALS AND METHOD

### A. Materials

Poly(dimethylsiloxane) (PDMS) (Sylgard 184, Dow Corning product) oligomer was used for making cross-linked blocks, within which microchannels were monolithically embedded. Flexible nylon monofilament (diameter: 530  $\mu\text{m}$  - 2 mm) procured from the local market was used for making templates for channel fabrication, and chloroform, purchased from Sigma-Aldrich, was used as a solvent for swelling the PDMS blocks. Room temperature vulcanizing silicone rubber (RTV1060A and its cross-linker) was purchased from Mingcheng Group Limited. A silicone tube (Sigma-Aldrich) of 2.0 mm ID was used for carrying the liquids. Silicone oil of viscosity 100 centistokes (cS) was purchased from M. R. Silicone Industries and was mixed with RTV at different weight ratios to reduce its viscosity. Oil-soluble dyes like Sudan Blue II and Oil Red O MS were procured from Sigma-Aldrich, and S. D. Fine Chem Limited and were used for making the dyed liquids.

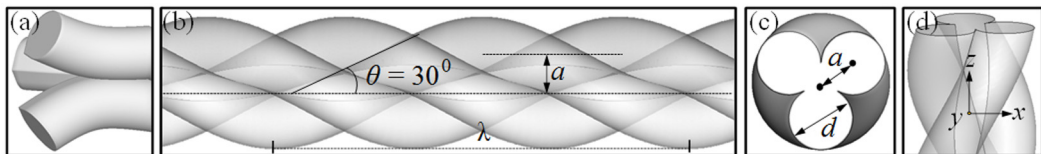


FIG. 1. (a), (b) Side view of three inlets and triple-helical microchannel, with helix angle  $\theta$ , helix radius  $a$ , and  $\lambda$ , defines the pitch or the wavelength of the channel. (c) The front view of the inlet of triple-helical channel. (d) A 3D view of the triple-helical channel.

### B. Method of preparation of microchannel embedded in PDMS blocks

Figure 1 shows the schematic of a triple-helical channel, which is characterized by three geometric features: helix radius  $a$ , helix angle  $\theta$ , and wavelength or helix pitch  $\lambda$ . These channels, embedded inside PDMS, were prepared by the method presented in Ref. [39]. In brief, a hand-operated mechanical device was designed for twisting three or more nylon strands to a desired helix angle. In order to make the twisted form permanent, it was first heated to  $\sim 100^\circ\text{C}$  and then cooled to room temperature. The hot set intertwined structure of three monofilaments as presented in Ref. [39] was used as the template. The template was placed inside a pool of PDMS (Sylgard 184, mixed with the cross-linker at 10:1 weight ratio) and was cross-linked to form a cuboid with the template embedded inside. The template was gently removed by pulling out the individual strands from the block preswelled with chloroform. The swollen block was then deswelled back by slowly drying off the solvent at a controlled condition. The channel thus formed consisted of three helical flow paths merged together forming a single channel, as shown in Fig. 2(a). The diameter of each helical flow path was varied from  $530 \pm 5 \mu\text{m}$  to  $1.8 \pm 0.1 \text{ mm}$  and the helix angle was varied from  $11^\circ \pm 0.5^\circ$  to  $36^\circ \pm 0.5^\circ$ . Since this channel was monolithically embedded inside the PDMS block, it was not possible to recover the solid mold generated inside [Fig. 2(a)]. Therefore, to facilitate access of the mold inside the channel, a sharp surgical blade was used to cut the PDMS block into two halves by driving it along the axis of the channel from the outlet to the inlet point where the three flow paths initially meet as shown in Figs. 2(b) and 2(c). For carrying out flow experiments, however, the channel needed to be closed, which was done by placing the two halves together with their matching surfaces pressed against each other by use of a binder clip as shown in Fig. 2(d). In this way, leakage of liquid from inside the channel was completely prevented.

### C. Method of preparation of dyed RTV liquids of different viscosity

The RTV liquid was white in color; therefore it was mixed with oil-soluble red and blue dyes to prepare mixing liquids of three different colors. In addition, the viscosity of the respective RTV liquids was to be reduced in order to increase the Reynolds number of flow. The dual objectives of coloring the RTV samples and reducing their viscosity were met in a two-step process. In the first step, the dye compounds, which were in the form of solid lumps, were first pulverized with a mortar and pestle and were then thoroughly mixed with the silicone oil of viscosity 100 cS. At the same time, the respective RTV liquids were mixed with the cross-linking agent (10:1, w/w). In the second step, the colored silicone oil was added to the RTV samples prepared earlier while also vigorously stirring the liquid mix. For the white RTV, the colorless silicone oil (without any dye) was mixed with the RTV sample. In order to attain different viscosities of RTV samples, silicone oil was added in a different weight ratio to it. For example, the viscosity of one such RTV sample (mixed with silicone oil) was found to be  $4.12 \text{ kg/m s}$  at shear rate  $= 1.25 \text{ s}^{-1}$ , while its density was  $\rho = 1250 \text{ kg/m}^3$  [40,41]. Considering the hydraulic diameter of the channels,  $d_h = 2.2 \text{ mm}$ , and flow rate of each liquid stream,  $Q = 4 \text{ ml/min}$ , the Reynolds  $\text{Re} = \bar{v}d_h\rho/\mu$  number was calculated as  $\text{Re} = 0.017$ . Thus, using RTV liquids of other different viscosity, the Reynolds number could be varied between  $\text{Re} = 4.23 \times 10^{-3}$  and 0.07. The minimum viscosity of RTV samples used in

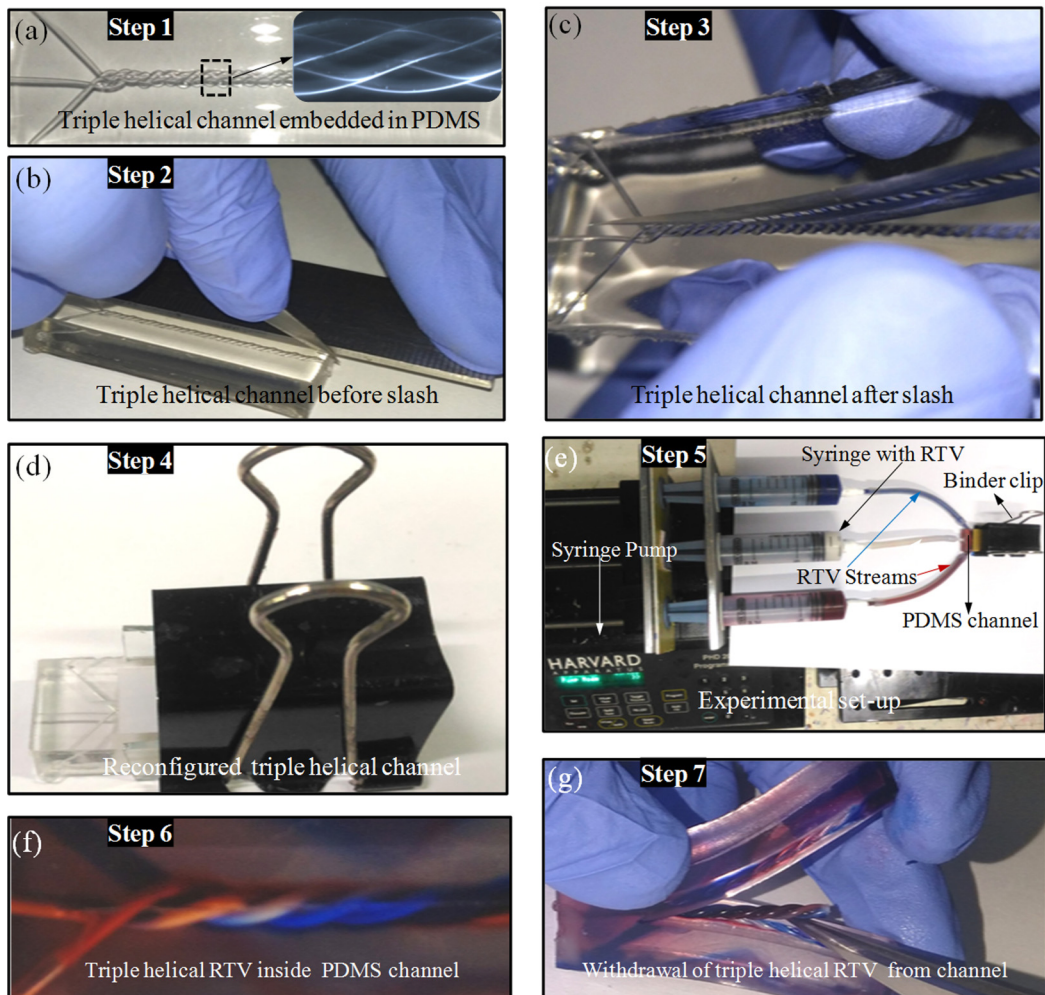


FIG. 2. (a) Optical micrograph shows a typical channel, embedded inside a PDMS block. (b)–(d) This block was incised along the channel axis to form two identical halves, which were placed with their matching surfaces pressed together with a binder clip. (e) Respective RTV streams mixed with the cross-linking agent (10:1, w/w); the dyes were pumped through three inlets of the channel for  $\sim 5$  min. (f), (g) Pumping of RTV was stopped and the PDMS block with RTV-filled channel was heated at  $60^\circ\text{C}$  inside a hot air oven for 10 min. Then the RTV was cross-linked inside the channel and the solid RTV mold was withdrawn by gently separating the two halves of the PDMS block.

the experiments was  $2.02\text{ kg/m.s}$ . Attempt to reduce viscosity further by the addition of silicone oil resulted in poor cross-linking of the RTV samples, which rendered them difficult to handle. The Reynolds number could not be increased further by increasing the flow rate because of leakage of liquid at a large pressure drop. The mixed liquids were kept inside a vacuum chamber to extract all the air from inside it. Following the removal of air bubbles, the RTV samples were poured into the syringes in such a way that no air could get trapped inside them.

#### D. Method of carrying out the experiment

All three syringes were then fitted in a syringe pump (Harvard apparatus, model PHD 2000 Infuse/withdraw); an outlet from each syringe was connected to three different inlets of the

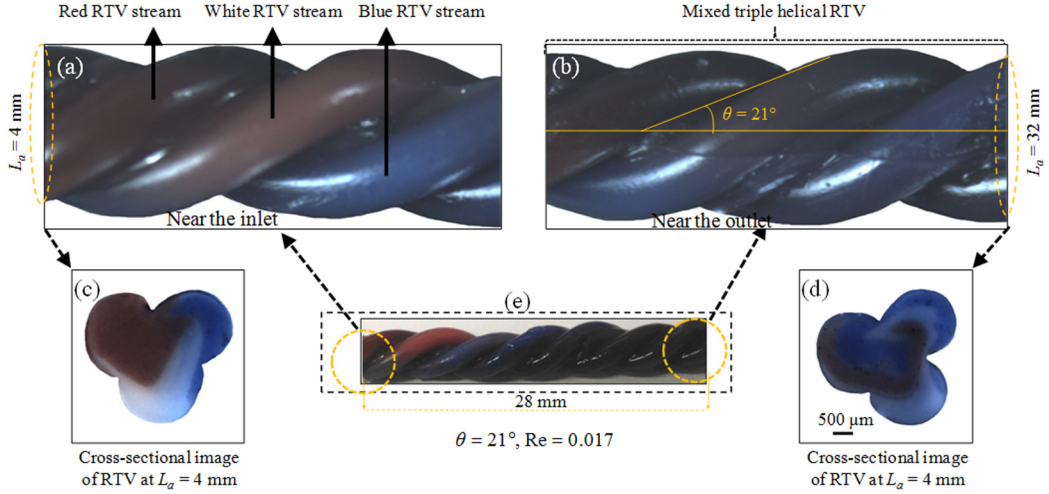


FIG. 3. (a), (b) Optical micrographs represent the side view of a typical RTV mold at the vicinity of the inlet of the channel and at an axial length of 32 mm from it. (c), (d) represent the cross sections of the RTV mold at 4 and 32 mm of axial length. A channel of helix angle  $\theta = 21^\circ$  and hydraulic diameter of  $\sim 2.2$  mm was used in the experiment. Reynolds number of flow was maintained at  $Re = 0.017$ .

microchannel by using a micropipet tip and silicone tube. The RTV streams from the three syringes were then pumped into three different lobes of the triple-helical channel through the three inlet tubes as shown in Fig. 2(e). The RTV was allowed to flow through the channel for about 10 min, following which the pumping of the liquid was stopped. The PDMS block was then placed inside a hot air oven at  $60^\circ\text{C}$  for  $\sim 10$  min, during which the RTV got cross-linked [Fig. 2(f)]. The binder clip, holding the two portions of the PDMS block, was then removed, and the RTV mold inside the channel was gently removed. It was taken for further analysis, as shown in Fig. 2(g). The RTV mold was cut into small parts of 2–4 mm length with their plane perpendicular to the axis of the channel. The image of the cross section of these RTV samples was captured using a charge-coupled device (CCD) camera to understand the extent of mixing of the three RTV streams at any given axial length of the channel.

### E. Calculation of mixing efficiency

Mixing efficiency was estimated by calculating the standard deviation in the intensity of color at any cross section of the channel. In particular, the intensity of the color for all pixels within a cross section was obtained. The standard deviation was then estimated as  $\sigma = \sqrt{\frac{1}{N} \sum_{i=0}^N (c_i - c_m)^2}$ , where  $N$  is the number of pixels and  $c_i$  represents the intensity of color at the  $i$ th pixel. The mean intensity, denoted by  $c_m$ , is calculated by finding the average intensity over all the pixels of the cross section. Mixing efficiency at a cross section is then written as  $\eta = (1 - \frac{\sigma}{\sigma_{\max}}) \times 100\%$ , where  $\sigma$  and  $\sigma_{\max}$  represent the standard deviation of concentration in a cross section at a given location and maximum standard deviation at the inlet, where the two liquids begin to mix.

## III. OBSERVATIONS

The optical images in Figs. 3(a)–3(d), show typical side and cross-sectional views of RTV samples collected from the inlet and the outlet of the channel, respectively. Here the flow rate of each liquid stream was maintained at  $Q = 4$  ml/min. The images show the presence of a sharp interface between the differently colored materials, suggesting that the dye molecules did not diffuse between different liquid streams.

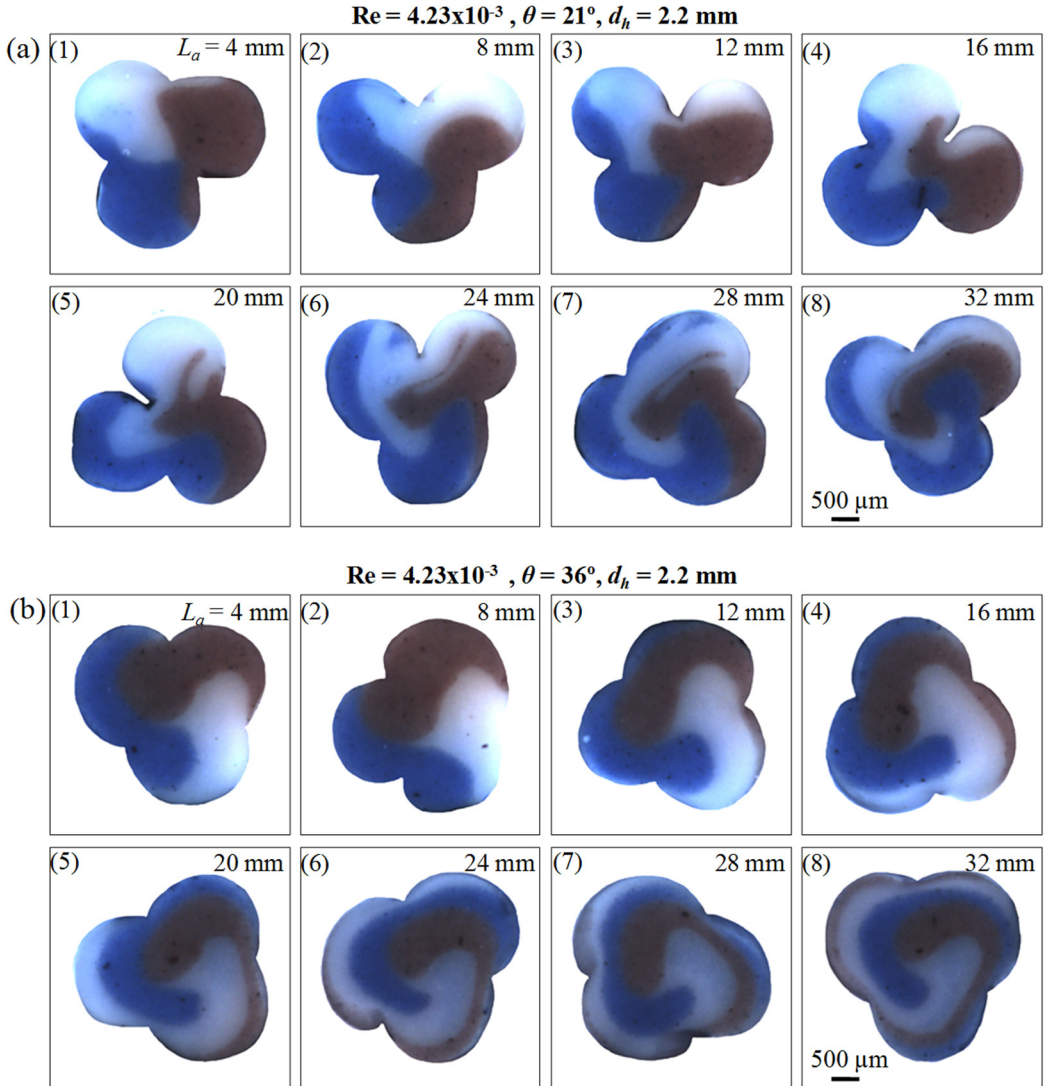


FIG. 4. (a), (b) Optical micrographs represent the cross section of the RTV mold for helix angle  $\theta = 21^\circ - 36^\circ$  at different axial lengths of 4–32 mm of the channel. The Reynolds number of flow is  $Re = 4.23 \times 10^{-3}$ .

Contours of mixing profile of three RTV streams for  $\theta = 21^\circ - 36^\circ$  and  $Re = 4.23 \times 10^{-3}$  are shown in Fig. 4; contours of mixing profile of three RTV streams for  $\theta = 21^\circ - 36^\circ$  and  $Re = 0.017$  are shown in Fig. 5.

In Figs. 4(a), 4(b), 5(a), and 5(b), we show optical images of cross sections of RTV mold at different axial lengths: 4–32 mm, for two different helix angles  $\theta = 21^\circ - 36^\circ$  and at a range of  $Re = 4.23 \times 10^{-3} - 0.017$ . Analysis of the images suggests that different kind of mixing interface patterns can be generated by varying the flow rates and helix angles. At constant Reynolds number, it is shown that the interface length of any stream of RTV gradually increases with an increase in helix angle from  $\theta = 21^\circ$  to  $36^\circ$  as shown in Figs. 4(a) and 4(b). On the other hand, at constant  $\theta = 21^\circ$ , for increase in Reynolds number:  $4.23 \times 10^{-3}$  to 0.017, at any cross section the length of the interface between different liquids increases with increase in penetration of one liquid into the other as shown in Figs. 4(a) (5–8) and 5(a) (4–8). At helix angle  $\theta = 36^\circ$ , and  $Re = 4.23 \times 10^{-3} - 0.017$ ,

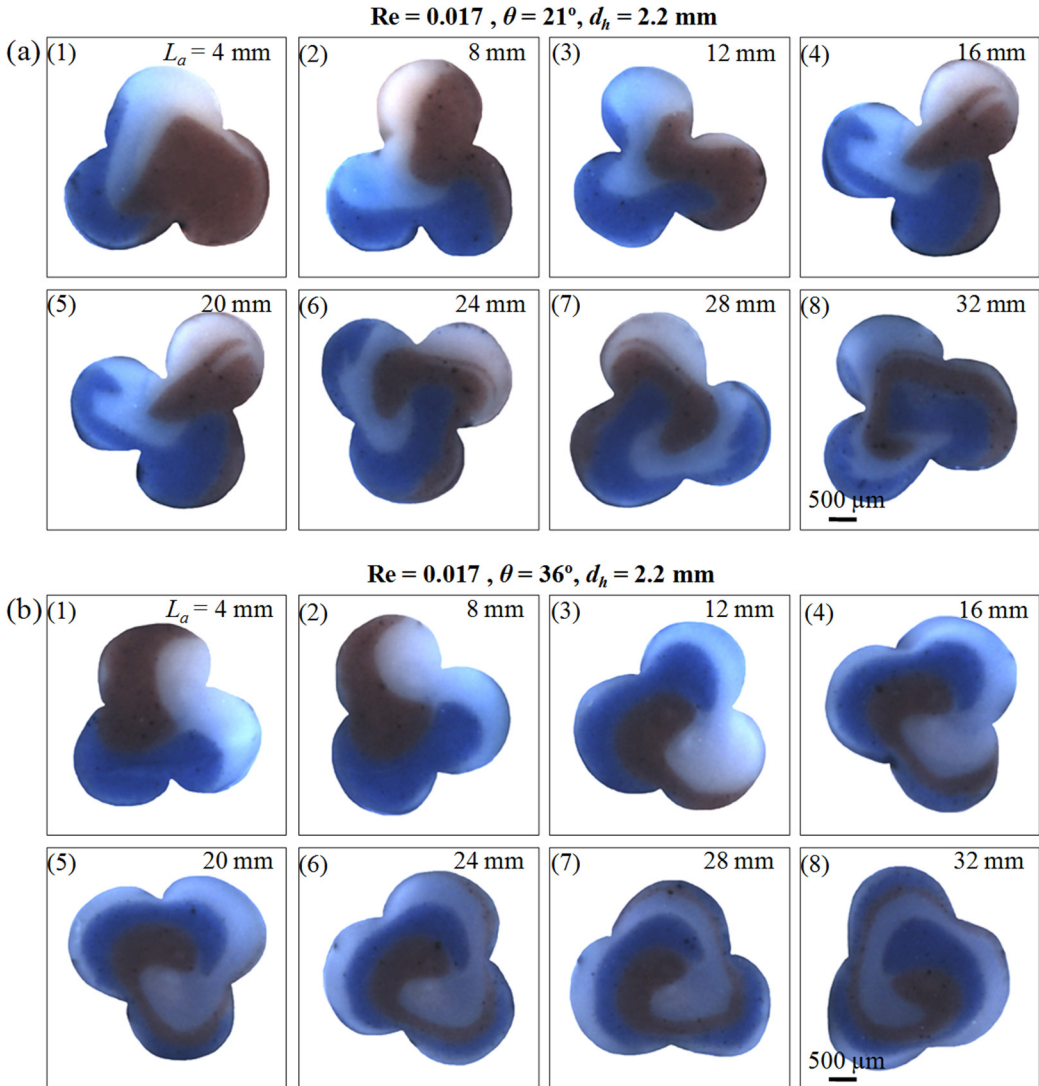


FIG. 5. (a), (b) Optical micrographs represent the cross section of the RTV mold for helix angle  $\theta = 21^\circ - 36^\circ$  at different axial lengths of 4–32 mm of the channel. The Reynolds number of flow is  $Re = 0.017$ .

the thickness of an individual RTV stream gradually decreases, and the length of the interface increases. These effects become more pronounced at even higher Reynolds number (Figs. S1(a) and S1(b) of the Supplemental Material [42]). In order to confirm that the observations made earlier occur irrespective of the liquid type, these experiments were repeated also with molten wax samples [43,44], which too showed similar behavior (Supplemental Material, Figs. S2(a)–S2(g), S3(a)–S3(e), and S4(a)–S4(c) [42]) although, because of experimental difficulties, a sharp image of the interface between three differently colored liquids could not be extracted. Thus, while the experiments yielded an excellent qualitative picture of the extent of mixing between different streams within a limited range of Reynolds number of flow, a more elaborate study was required to have a quantitative effect of different parameters on mixing within the microchannel. It is for this purpose that 3D simulation of this phenomenon was carried out using FLUENT software.

### A. Channel dimension considered for carrying out flow simulation

The helix angle of triple-helical channels, as shown in Fig. 1, was considered to vary from  $\theta = 6^\circ$  to  $34^\circ$ . The flow area of the channel is  $A_s = 2.4d^2$ , and the wetted perimeter is  $W_L = 7.85d$ . Therefore, the hydraulic radius can thus be represented as  $d_h = 4A_s/W_L \sim 1.22d$ . For the purpose of flow simulation, the diameter of individual helical flow paths was considered to be  $50 \mu\text{m}$ , so that the helix radius  $a$  for all our channels was  $\sim 29 \mu\text{m}$  and the hydraulic diameter was estimated to be  $\sim 61 \mu\text{m}$ . The axial length of the channel was maintained at 2 mm for all simulations.

### B. Numerical simulation

The method of generation of computational grids has been described in detail in Rajbanshi and Ghatak [45] and is briefly presented in the Supplemental Material, T1 [42]. Governing equations and solver settings for 3D simulation of flow and species transport have also been illustrated in T2 in the Supplemental Material [42].

## IV. RESULTS AND DISCUSSION

In simulation, two different model liquids, water (density,  $\rho$ : 998.2 kg/m<sup>3</sup>; viscosity,  $\mu$ : 0.001 kg/m s; and molecular weight,  $M_w$ : 18.01 kg/kmol) and acetone (density,  $\rho$ : 791 kg/m<sup>3</sup>; viscosity,  $\mu$ : 0.000331 kg/m s; and molecular weight,  $M_w$ : 58.01 kg/kmol), were used for studying mixing at different Reynolds numbers of flow and the helix angle. These two liquids are completely miscible, and therefore the mass diffusivity between these two liquids is known to be  $4.65 \times 10^{-9}$  [46]. However, to unravel the role of secondary circumferential flow in generating the chaotic advection (Jones *et al.* [47]; Aref [48]) and the resultant folded structure (Jones *et al.* [47]) of the two liquids, it was assumed that the diffusivity between these two liquids is very small. In particular, the calculations were done at two different diffusion coefficients,  $D = 10^{-10} \text{ m}^2/\text{s}$  and  $D = 10^{-20} \text{ m}^2/\text{s}$ . At such small values of  $D$ , the interface between the two liquids is expected to be sharp, and the mixing is primarily expected to occur via an increase in the interfacial area between the two liquid streams.

### A. Contours of mixing profile of acetone and water for different $\theta$ and Re

In Fig. 6, we present the simulated contour profiles of these two liquids at different cross sections along the length of the channel. The results represent channels with two different helix angles,  $\theta = 16^\circ$  and  $34^\circ$ , with Reynolds number of flow maintained at  $\text{Re} = 24.6$ ; the diffusivity between the two liquids was considered to be  $D = 10^{-10} \text{ m}^2/\text{s}$ . For each sequence, the images represent the extent of mixing at different axial lengths of the channel. Results for other helix angles and Reynolds number of flow are presented in Figs. S5(a)–S5(f) of the Supplemental Material [42]. These images are analyzed to obtain the mixing efficiency between the two liquids. In Figs. S6(a)–S6(d) we present the variation of mixing efficiency,  $\% \eta$  at different axial lengths  $L_a$  of the channel at a range of  $\text{Re} = 0.025$ –246 and helix angle  $\theta = 6^\circ$ – $34^\circ$ .

In Fig. 7(a) we present the mixing efficiency  $\% \eta$  against the Reynolds number  $\text{Re}$  for different helix angles,  $\theta = 6^\circ$ – $34^\circ$ . In each case,  $\% \eta$  was calculated for an axial length of  $L_a = 2 \text{ mm}$  following the procedure described earlier. For each helix angle,  $\% \eta$  was found to vary nonmonotonically with  $\text{Re}$ , suggesting the occurrence of two different phenomena. This results corroborates with similar observations in the context of mixing in Verma *et al.* [49], Jiang *et al.* [38], Liu *et al.* [32], and Jani *et al.* [50]. It is concluded that at smaller values of  $\text{Re}$ , diffusion of liquids across the interface between them can occur over long residence time; as a result mixing efficiency remains large [51,52]. However, with increase in  $\text{Re}$ , the time available for such transport of mass over a given length  $L$  of the channel diminishes; with it, the mixing efficiency  $\% \eta$  also decreases. The relative effect of diffusion time and that for convection or the residence time on mixing efficiency is expressed by the dimensionless Péclet number,  $\text{Pe} = \bar{v}L/D$  where  $L$  is the given axial

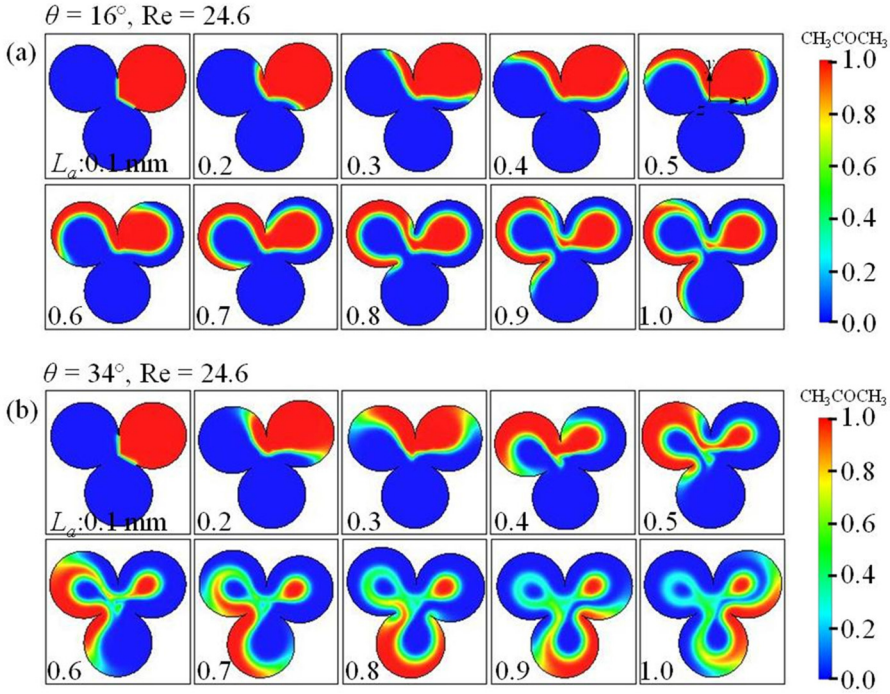


FIG. 6. Contour profiles of mixing of acetone and water flowing at different Reynolds numbers in triple-helical channels of different helix angles. (a), (b) Contour profiles are captured at varying axial length in channels with helix angle  $\theta = 16^\circ$  and  $34^\circ$ , respectively, at Reynolds number  $Re = 24.6$ . These calculations were carried out by considering the diffusivity between two liquids as  $D = 10^{-10} \text{ m}^2/\text{s}$ .

length of the channel. Mixing efficiency  $\% \eta$  decreases with increase in the Péclet number of flow through a channel. The Péclet number can be further written as a product of the Reynolds number ( $Re_L$ ) calculated with axial length  $L$  of the channel as the characteristic length and the Schmidt

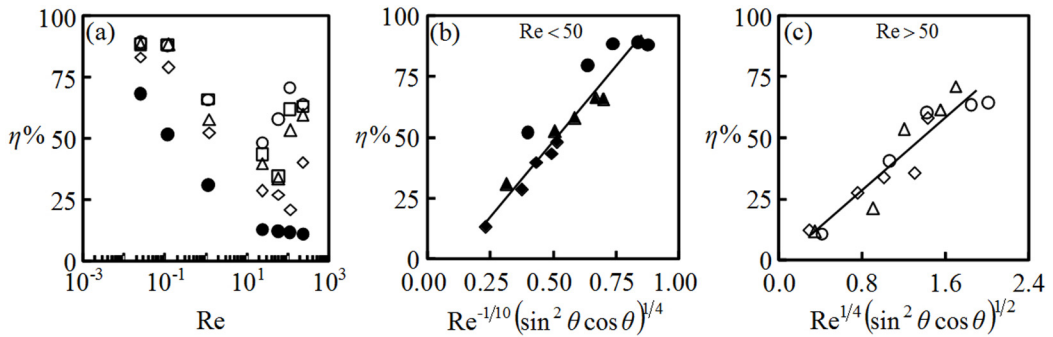


FIG. 7. Mixing efficiency of contour plots obtained from simulation. (a) The mixing efficiency  $\% \eta$  is calculated from contour plots, like the ones presented in Figs. 6 and S5 and several others simulated for different values of  $Re$  and  $\theta$ , and is plotted against Reynolds number of flow. The symbols  $\bullet$ ,  $\diamond$ ,  $\Delta$ ,  $\square$ , and  $\circ$  represent data for helix angles  $\theta = 6^\circ$ ,  $16^\circ$ ,  $22^\circ$ ,  $30^\circ$ , and  $34^\circ$ , respectively. (b), (c) The plots show that  $\% \eta$  scales differently for different ranges of  $Re$ :  $Re < 50$  and  $Re > 50$ . Here the symbols  $\bullet$ ,  $\blacktriangle$ , and  $\blacklozenge$  represent  $Re = 0.123$ ,  $1.23$ ,  $24.6$  and  $\circ$ ,  $\Delta$ , and  $\diamond$  represent  $Re = 246$ ,  $123$ , and  $61.5$ , respectively.

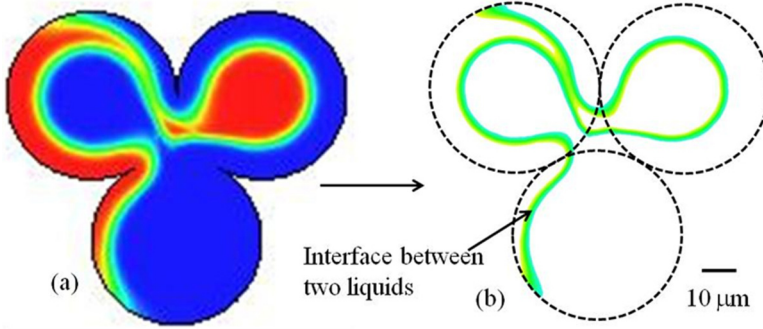


FIG. 8. (a), (b) Image of a typical cross section of the microchannel in which two different liquids are pumped. The line representing the interface between the two liquids is extracted using image processing software. The contour length  $L_c$  of the interface was then calculated.

number:  $Pe = (L\bar{v}\rho/\mu)(\mu/\rho D) = Re_L Sc$ . Noting that  $Re_L \sim (L/d)Re$ , the Péclet number can be expressed as  $Pe = (L/d)ReSc$ . In our experiments both the  $L/d$  ratio and the Schmidt number  $Sc$  remain unaltered, so at smaller values of  $Re$ ,  $\eta\%$  decreases with increase in  $Pe$ . A different phenomenon sets in at larger  $Re$ . With increase in  $Re$ , the secondary flow at the cross section of the channel becomes strong with the result that the interfacial area between the two liquids increases, concomitant to  $\eta\%$  also increasing. Quantitative analysis of dependence of  $\eta\%$  on  $Re$  and  $\theta$  captures these results as presented in Figs. 7(b) and 7(c). Here, mixing efficiency  $\eta\%$  varies differently at two different ranges of  $Re$ : at  $Re < 50$ ,  $\eta\% \sim Re^{-1/10}(\sin^2\theta \cos\theta)^{1/4}$  and at  $Re > 50$ ,  $\eta\% \sim Re^{1/4}(\sin^2\theta \cos\theta)^{1/2}$ . Flow in helical channels has earlier been shown to be mediated by two different dimensionless numbers: the Dean number  $Dn = Re(a\kappa)^{0.5}$  and the Germano number,  $Gn = Re(a\tau)$ ; one accounts for the curvature,  $a\kappa = \sin^2\theta$ , of the helix and the other takes into account the effect of its torsion,  $a\tau = \sin\theta \cos\theta$ . For a planar spiral tube with negligible torsion, the flow is essentially determined by the Dean number,  $Dn$ . However, with increase in torsion, as with a single helical coil, the effect of torsion increases, so that the flow within such channel begins to be determined by both these parameters. As a first approximation, for larger  $Re$ ,  $Re > 50$ , the flow can be thought to be determined by the geometric mean of the above two numbers:  $(GnDn)^{1/2} \sim Re(\sin^2\theta \cos\theta)^{1/2}$ . In the context of mixing between fluids, the mixing efficiency  $\eta\%$  depends also on the Péclet number  $Pe$ , such that with increase in  $Pe$ ,  $\eta\%$  decreases. It has been shown in different contexts that  $\eta\%$  does not vary exactly linearly with  $Pe^{-1}$ , but sublinearly [53,54], e.g.,  $\eta\% \sim Pe^{-m}$ , where the exponent  $m$  has been shown to vary from 0.6 to 0.8. Hence, combining these effects and considering that  $m \sim 0.75$ , the mixing efficiency  $\eta\%$  is indeed found to scale as  $\eta\% \sim (GnDn)^{1/2}/Pe^{0.75} \sim Re^{0.25}(\sin^2\theta \cos\theta)^{1/2}$ , which corroborates with that estimated from the simulation results. At smaller value of  $Re$ , e.g.,  $Re < 50$ , the dependence of flow on the helix angle is expected to be less pronounced, such that the dependence of  $\eta\%$  on  $Gn$  and  $Dn$  can be written as  $(GnDn)^{1/4}$ , leading to a relation for  $\eta\%$  as  $\eta\% \sim (GnDn)^{1/4}/Pe^{0.75} \sim Re^{-0.25}(\sin^2\theta \cos\theta)^{1/4}$ ; in analysis from simulation,  $\eta\% \sim Re^{-0.1}$ , possibly because of a slightly different value of exponent  $m$ .

### B. Length of interface between two liquids

Since the extent of mixing depends on the area of the interface between the two liquids, it is worth quantifying the stretching and thickening of the interface as a function of geometric parameters and the Reynolds number of flow. The image in Figs. 8(a) and 8(b) shows the state of mixing between the two liquids at a typical cross section, the interface between which was extracted out using image processing software IMAGEJ. In order to detect the interface, RGB color intensities (25, 182, 253) to (165, 254, 26) were considered to form the interface region. These data, presented in Figs. 9–12,

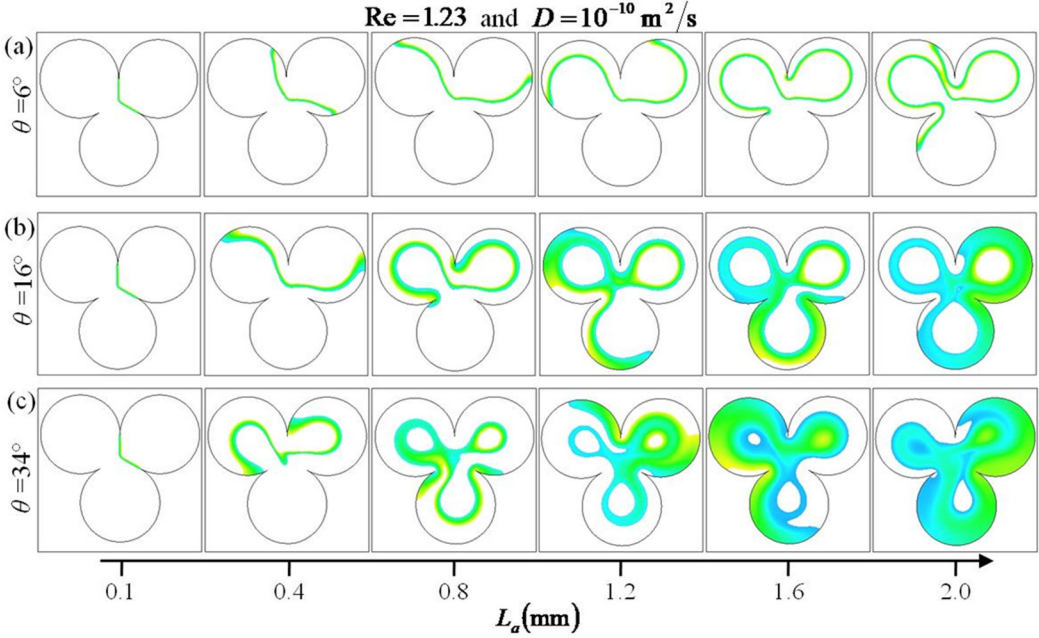


FIG. 9. The sequence of images represents calculations carried out for diffusivity  $D = 10^{-10} \text{ m}^2/\text{s}$  between the liquids which were pumped into channels of helix angle  $\theta = 6^\circ - 34^\circ$  at Reynolds number  $\text{Re} = 1.23$ .

show that at the inlet of the channel the length of the interface is minimum, but with an increase in its axial length the contour length of the interface increases. In fact, the interface undergoes stretching, folding, and also thickening. The effect of thickening of the interface gets more pronounced at a larger helix angle as shown in Fig. 9(c) for  $\theta = 34^\circ$ . For such interfaces, calculation of the length of the interface tends to get less accurate. Hypothesizing that such thickening of the interface happens because of diffusion between the two liquids, the effect of diffusion was required to be minimized. Thus, to capture the sole effect of hydrodynamics on the deformation of the interface, calculations were carried out at a reduced diffusivity of  $D = 10^{-20} \text{ m}^2/\text{s}$  [55,56]. These results are presented in Fig. 10 in which the evolution of the interface in channels with three different helix angles,  $\theta = 6^\circ$ ,  $16^\circ$ , and  $34^\circ$  and Reynolds number  $\text{Re} = 1.23$  is presented. Examination of the images in Figs. 10, 11(a) and 11(b) shows that at large Reynolds number, e.g.,  $\text{Re} = 123$ , and high helix angle, e.g.,  $\theta = 22^\circ$  and  $34^\circ$ , the interface undergoes not only stretching and folding but also apparent coalescence with an existing portion of the interface and even branching. Notably, coalescence and branching are not observed for smaller  $\theta$  even at large Reynolds number. Comparison of calculations with  $D = 10^{-10} \text{ m}^2/\text{s}$  and  $D = 10^{-20} \text{ m}^2/\text{s}$  at  $\text{Re} = 123$  (Fig. 12) show that thickening of the interface occurs not because of diffusion of mass but because of these additional effects not observed for other similar microchannels reported in the literature, e.g., the spiral channel and the ones decorated with the herringbone pattern at the wall [8,57].

Both the contour length of the interface and its area were obtained by image processing. In Fig. 13(a) we plot the contour  $L_c$  against the axial length  $L_a$  of the channel for different  $\theta$  and  $\text{Re}$ . The data show that at a smaller helix angle,  $\theta = 6^\circ$ ,  $L_c$  varies almost similarly with  $L_a$  for different  $\text{Re}$ ; however, for higher helix angle,  $\theta = 34^\circ$ ,  $L_c$  remains larger for higher values of  $\text{Re}$ . The stretching of the interface can be examined in the light of nonlinear stability analysis in which an error parameter increases exponentially with time (Villermaux *et al.* [58]). In the laminar regime considered here, the flow field and the resultant extent of mixing between fluids remain constant with respect to time. Nevertheless, the length of the interface increases with the axial length of the

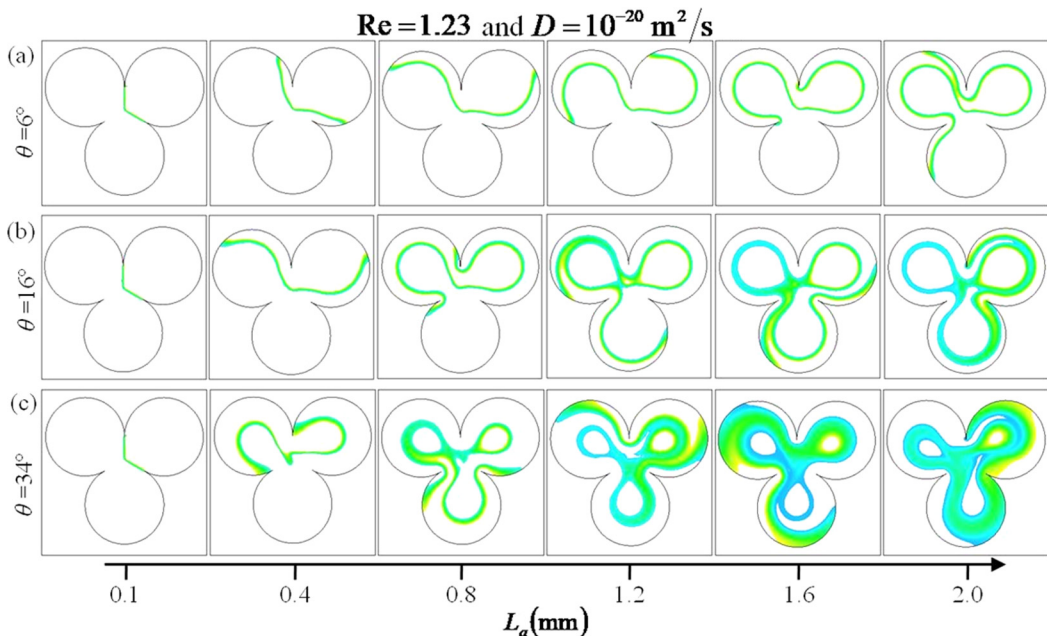


FIG. 10. (a)–(c) The sequence of images represents calculations carried out for diffusivity  $D = 10^{-20} \text{ m}^2/\text{s}$  between two liquids which were pumped into channels of helix angle  $\theta = 6^\circ - 34^\circ$  at Reynolds number  $Re = 1.23$ .

channel, which can be quantified by the Lyapunov exponent defined as [23,32]

$$p = \lim_{L_a \rightarrow \infty} \frac{1}{L_a} \ln \left( \frac{L_c|_f}{L_c|_0} \right),$$

where  $L_c|_0$  and  $L_c|_f$  represent, respectively, the contour length of the interface at the beginning and end of the channel. Notice that in the definition of  $p$ , we have replaced time by the axial length  $L_a$ . It is worth noting also that  $L_a$  does not exactly increase to  $\infty$  but to  $2 \text{ mm} \gg d_h = 61 \mu\text{m}$ ; beyond  $L_a = 2 \text{ mm}$ , instead of stretching, coalescence of interface occurs. Analysis of Lyapunov exponent  $p$  for different data sets shows that  $p$  varies only weakly with  $Re$  in the range considered but varies significantly with helix angle  $\theta$ . The inset of Fig. 13(a) shows that  $p$  obtained from different sets of parameters all fall on a master line when plotted against the quantity  $(\sin^2 \theta \cos \theta)$ . The error bars in the data represent the standard deviation for Reynolds number varying over two orders of magnitude. This result corroborates with that of others in the literature (Sawyers *et al.* [59], Niu and Lee [60], Xia *et al.* [23], and Liu *et al.* [32]) where too, the Lyapunov exponent was found to be weakly dependent on  $Re$  within some range. However, for the triple-helical channel,  $p$  was significantly larger than obtained by others within a large range of Reynolds numbers.

Similar to the contour length of the interface, its area  $A_c$  was also obtained for a range of helix angle of channel and Reynolds number of flow. The data presented in Fig. 13(b) show that  $A_c$  increases linearly with the axial length of the channel, but with respect to the helix angle, it varies as  $A_c \sim (\sin^2 \theta \cos \theta)^{1/2}$ .

## V. SUMMARY

We have presented a systematic experimental and theoretical study of mixing of two different liquids within triple-helical microchannels. Our calculations have shown that at large helix angle, the effect of the secondary circumferential flow becomes strong enough that the interface, through

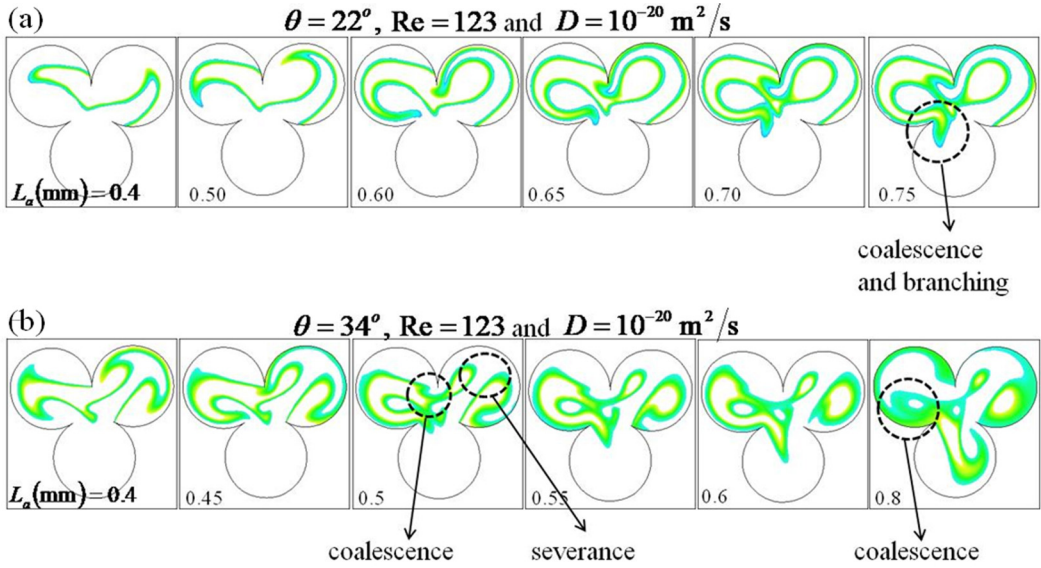


FIG. 11. (a), (b) The sequence of images depicts coalescence and branching of the interface for two different sets of parameters.

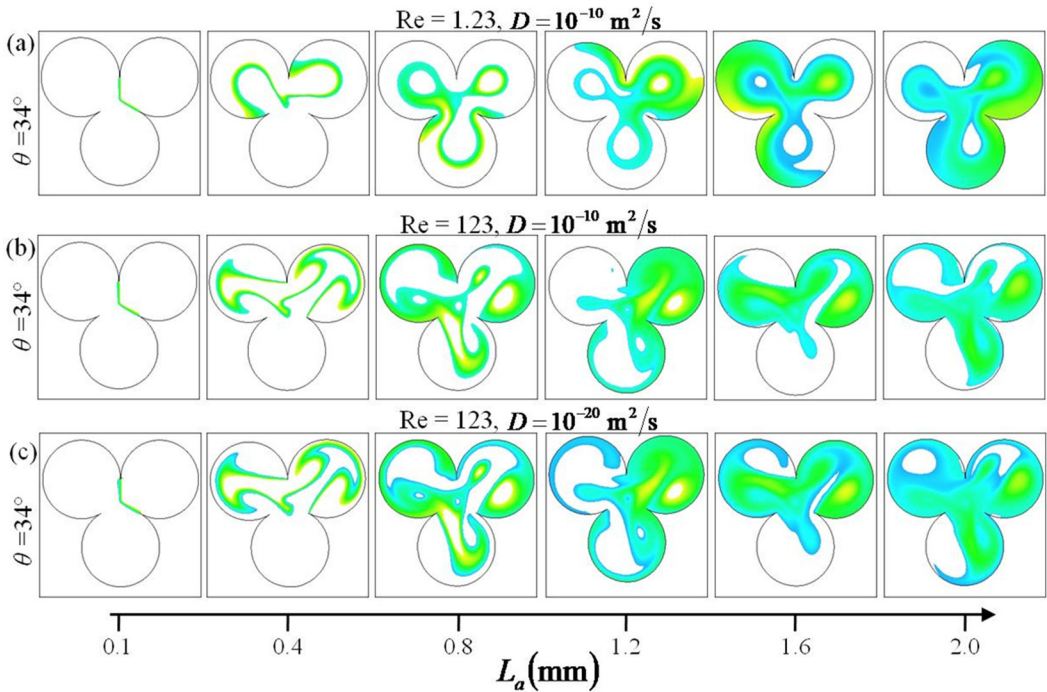


FIG. 12. (a), (b) The sequence of images represents calculations carried out for diffusivity  $D = 10^{-10} \text{ m}^2/\text{s}$  between the liquids which were pumped into a channel of helix angle  $\theta = 34^\circ$  at Reynolds numbers  $Re = 1.23$  and  $123$ , respectively. (c) The calculations as in (b) were repeated for diffusivity  $D = 10^{-20} \text{ m}^2/\text{s}$ .

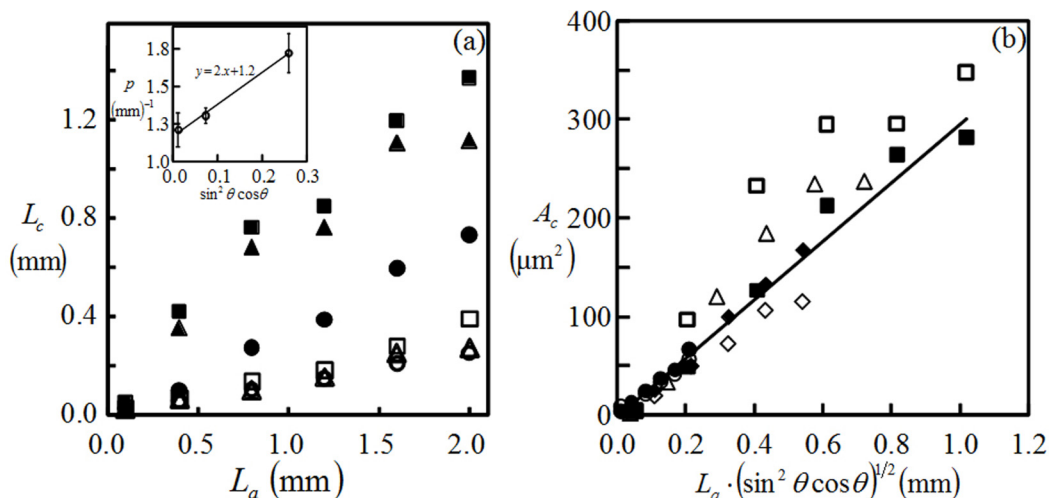


FIG. 13. (a)  $L_c$  data from different set of parameters were plotted against axial length  $L_a$ . The symbols  $\circ$ , and  $\triangle$  represent flow through channels of helix angle  $\theta = 6^\circ$  at Reynolds numbers 1.23, 24.6, and 123, respectively; the symbols  $\bullet$ ,  $\blacksquare$ , and  $\blacktriangle$  represent  $\theta = 34^\circ$  and  $\text{Re} = 1.23$ , 24.6, and 123, respectively. The inset shows the Lyapunov exponent as calculated for different  $\theta$  and  $\text{Re}$ , and plotted against the quantity  $\sin^2 \theta \cos \theta$ . (b) The estimated area of the interface is plotted against  $L_a (\sin^2 \theta \cos \theta)^{1/2}$ . The symbols  $\circ$ ,  $\diamond$ ,  $\triangle$ , and  $\square$  represent  $\theta = 6^\circ$ ,  $16^\circ$ ,  $22^\circ$ , and  $34^\circ$ , respectively. Open and filled symbols represent  $\text{Re} = 123$  and 1.23, respectively.

which the mass transfer can occur, increases significantly. The mixing efficiency between two different streams is shown to scale linearly with the geometric mean of the Dean number and the Germano number  $\% \eta \sim (\text{DnGn})^{1/2} \sim (\sin^2 \theta \cos \theta)^{1/2}$ . From the contour length of the interface of the two liquids, we have obtained also the Lyapunov exponent  $p$ , which defines the rate at which an initial contact between the two streams gets stretched over the axial length of the channel. Our calculations show that this rate depends strongly on the geometry of the triple helix,  $p \sim \sin^2 \theta \cos \theta$ , remaining independent over a large range of Reynolds number of the flow. The Lyapunov exponent was also significantly larger than that reported by others in the literature suggesting strong chaotic advection. Thus combining the scaling relations for  $\% \eta$  and  $p$ , respectively, the mixing efficiency  $\% \eta$  is found to scale with the Lyapunov exponent as  $\% \eta \sim p^{1/2}$ . Geometry mediated occurrence of a very large value of Lyapunov exponent suggests rapid mixing between liquids. It is worth pointing out that the Lyapunov exponent could be estimated over a length scale of a conventional helical mixer, which was smaller than that in the experiment.

#### ACKNOWLEDGMENTS

A.G. acknowledges the Department of Science and Technology, Government of India, for financial assistance in the form of Grant No. DST/CHE/20080165 and the DST grant under the FIST Program 2013.

- [1] D. R. Reyes, D. Iossifidis, P. Auroux, and A. Manz, Micro total analysis systems. I. Introduction, theory, and technology, *Anal. Chem.* **74**, 2623 (2002).
- [2] P. A. Auroux, D. R. Reyes, D. Iossifidis, and A. Manz, Micro total analysis systems. II. Analytical standard operations and applications, *Anal. Chem.* **74**, 2637 (2002).

- [3] S. L. Stott, C. H. Hsu, D. I. Tsukrov, M. Yu, D. T. Miyamoto, B. A. Waltman, S. M. Rothenberg, A. M. Shah, M. E. Smas, G. K. Korir, and F. P. Floyd, Isolation of circulating tumor cells using a microvortex-generating herringbone-chip, *Proc. Natl. Acad. Sci. USA* **107**, 18392 (2010).
- [4] M. A. Burns, B. N. Johnson, S. N. Brahmamandra, K. Handique, J. R. Webster, M. Krishnan, T. S. Sammarco, P. M. Man, D. Jones, D. Heldsinger, C. H. Manstrangelo, and D. T. Burke, An integrated nanoliter DNA analysis device, *Science* **282**, 484 (1998).
- [5] J. Eiali, S. Gaudet, A. Gunther, P. K. Sorger, and K. F. Jensen, Cell stimulus and lysis in a microfluidic device with segmented gas-liquid flow, *Anal. Chem.* **77**, 3629 (2005).
- [6] B. N. Kholodenko, O. V. Demin, G. Moehren, and J. B. Hoek, Quantification of short term signalling by the epidermal growth factor receptor, *J. Biol. Chem.* **274**, 30169 (1999).
- [7] A. Blau, Cell adhesion promotion strategies for signal transduction enhancement in microelectrode array in vitro electrophysiology: An introductory overview and critical discussion, *Curr. Opin. Colloid Interface Sci.* **18**, 481 (2013).
- [8] A. D. Stroock, S. K. Dertinger, A. Ajdari, I. Mezić, H. A. Stone, and G. M. Whitesides, Chaotic mixer for microchannels, *Science* **295**, 647 (2002).
- [9] F. Schönfeld and S. Hardt, Simulation of helical flows in microchannels. *AIChE J.* **50**, 771 (2004).
- [10] D. Therriault, S. R. White, and J. A. Lewis, Chaotic mixing in three-dimensional microvascular networks fabricated by direct-write assembly, *Nat. Mater.* **2**, 265 (2003).
- [11] D. Rothstein, E. Henry, and J. P. Gollub, Persistent patterns in transient chaotic fluid mixing, *Nature* **401**, 770 (1999).
- [12] S. W. Jones and W. R. Young, Shear dispersion and anomalous diffusion by chaotic advection, *J. Fluid Mech.* **280**, 149 (1994).
- [13] S. R. Ganneboyina and A. Ghatak, Multi-helical micro-channels for rapid generation of drops of water in oil, *Microfluid Nanofluid.* **15**, 637 (2013).
- [14] T. Eisner, *For Love of Insects* (Belknap Press of Harvard University Press, Cambridge, MA, 2003).
- [15] T. J. Ober, D. Foresti, and J. A. Lewis, Active mixing of complex fluids at the microscale, *Proc. Natl. Acad. Sci. USA* **112**, 12293 (2015).
- [16] D. Bothe, C. Stemich, and H. J. Warnecke, Fluid mixing in a T-shaped micro-mixer, *Chem. Eng. Sci.* **61**, 2950 (2006).
- [17] N. A. Mouheb, D. Malsch, A. Montillet, C. Sollicc, and T. Henkel, Numerical and experimental investigations of mixing in T-shaped and cross-shaped micromixers, *Chem. Eng. Sci.* **68**, 278 (2012).
- [18] K. Sriharan, C. J. Strobl, M. F. Schneider, A. Wixforth, and Z. V. Guttenberg, Acoustic mixing at low Reynold's numbers, *Appl. Phys. Lett.* **88**, 054102 (2006).
- [19] I. Glasgow and N. Aubry, Enhancement of microfluidic mixing using time pulsing, *Lab Chip* **3**, 114 (2003).
- [20] J. Marschewski, S. Jung, P. Ruch, N. Prasad, S. Mazzotti, B. Michel, and D. Poulidakos, Mixing with herringbone-inspired microstructures: Overcoming the diffusion limit in co-laminar microfluidic devices, *Lab Chip* **15**, 1923 (2015).
- [21] S. W. Lee, D. S. Kim, S. S. Lee, and T. H. Kwon, A split and recombination micromixer fabricated in a PDMS three-dimensional structure, *J. Micromech. Microeng.* **16**, 1067 (2006).
- [22] F. Schönfeld, V. Hessel, and C. Hofmann, An optimised split-and-recombine micro-mixer with uniform 'chaotic' mixing, *Lab Chip* **4**, 65 (2004).
- [23] H. M. Xia, C. Shu, S. Y. M. Wan, and Y. T. Chew, Influence of the Reynolds number on chaotic mixing in a spatially periodic micromixer and its characterization using dynamical system techniques, *J. Micromech. Microeng.* **16**, 53 (2005).
- [24] H. Sato, S. Ito, K. Tajima, N. Orimoto, and S. Shoji, PDMS microchannels with slanted grooves embedded in three walls to realize efficient spiral flow, *Sens. Actuators, A* **119**, 365 (2005).
- [25] N. S. Lynn and D. S. Dandy, Geometrical optimization of helical flow in grooved micromixers, *Lab Chip* **7**, 5802007.
- [26] A. P. Sudarsan and V. M. Ugaz, Multivortex micromixing, *Proc. Natl. Acad. Sci. USA* **103**, 7228 (2006).
- [27] W. R. Dean, Note on the motion of fluid in a curved pipe, *Philos. Mag.* **4**, 208 (1927).
- [28] M. Germano, On the effect of torsion on a helical pipe flow, *J. Fluid Mech.* **125**, 1 (1982).

- [29] H. C. Kao, Torsion effect on fully developed flow in a helical pipe, *J. Fluid Mech.* **184**, 335 (1987).
- [30] S. Murata, Y. Miyake, T. Inaba, and H. Ogawa, Laminar flow in a helically coiled pipe, *Bull. JSME* **24**, 355 (1981).
- [31] J. M. T. Thompson and A. R. Champneys, From helix to localized writhing in the torsional post-buckling of elastic rods, *Local. Solit. Waves Solid Mech.* **12**, 111 (1999).
- [32] K. Liu, Q. Yang, F. Chen, Y. Zhao, X. Meng, C. Shan, and Y. Li, Design and analysis of the cross-linked dual helical micromixer for rapid mixing at low Reynolds numbers, *Microfluid. Nanofluid.* **19**, 169 (2015).
- [33] M. Khoshvaght-Aliabadi, Z. Arani, and F. Rahimpour, Influence of  $\text{Al}_2\text{O}_3\text{-H}_2\text{O}$  nanofluid on performance of twisted minichannels, *Adv. Powder Technol.* **27**, 1514 (2016).
- [34] S. R. Ganneboyina and A. Ghatak, Generation of air-water two-phase flow patterns by altering the helix angle in triple helical microchannels, *Ind. Chem. Res.* **51**, 9356 (2012).
- [35] C. J. Bolinder, The effect of torsion on the bifurcation structure of laminar flow in a helical square duct, *J. Fluids Eng.* **117**, 242 (1995).
- [36] G. Wölk, M. Dreyer, and H. J. Rath, Flow patterns in small diameter vertical non-circular channels, *Int J. Multiphase Flow* **26**, 1037 (2000).
- [37] G. B. Salieb-Beugelaar, D. Gonçalves, M. Wolf, and P. Hunziker, Microfluidic 3D helix mixers, *Micromachines* **7**, 189 (2016).
- [38] F. Jiang, K. S. Drese, S. Hardt, M. Küpper, and F. Schönfeld, Helical flows and chaotic mixing in curved micro channels, *AIChE J.* **50**, 2297 (2004).
- [39] M. K. S. Verma, A. Majumder, and A. Ghatak, Embedded template assisted fabrication of complex microchannels in PDMS and design of a micro-fluidic adhesive, *Langmuir* **22**, 10291 (2006).
- [40] S. E. Shim and A. I. Isayev, Rheology and structure of precipitated silica and poly (dimethyl siloxane) system. *Rheol. Acta* **43**, 127 (2004).
- [41] L. Lei, W. Xishan, and C. Dengke, Corona ageing tests of RTV and RTV nanocomposite materials, *ICSD* **2**, 804 (2004).
- [42] See Supplemental Material at <http://link.aps.org/supplemental/10.1103/PhysRevFluids.5.064502> for supplemental texts and images.
- [43] R. Longworth and W. F. Busse, Melt-viscosity relationships for molten polyethylene-paraffin wax mixtures, *Trans. Soc. Rheol.* **6**, 179 (1962).
- [44] H. Inaba and P. Tu, Evaluation of thermophysical characteristics on shape-stabilized paraffin as a solid-liquid phase change material, *Heat Mass Transfer* **32**, 307 (1997).
- [45] P. Rajbanshi and A. Ghatak, Flow through triple helical microchannel, *Phys. Rev. Fluids* **3**, 024201 (2018).
- [46] T. Grossmann and J. Winkelmann, Ternary diffusion coefficients of glycerol+ acetone+ water by Taylor dispersion measurements at 298.15 K, *J. Chem. Eng. Data* **50**, 1396 (2005).
- [47] S. W. Jones, O. M. Thomas, and H. Aref, Chaotic advection by laminar flow in a twisted pipe, *J. Fluid Mech.* **209**, 335 (1989).
- [48] H. Aref, Chaotic advection of fluid particles, *Philos. Trans. of the Royal Soc. of London, Ser. A: Phys. and Eng. Sci.* **333**, 273 (1990).
- [49] M. K. S. Verma, S. R. Ganneboyina, R. Vinayak, and A. Ghatak, Three-dimensional multihelical microfluidic mixers for rapid mixing of liquids, *Langmuir* **24**, 2248 (2008).
- [50] J. M. Jani, M. Wessling, and R. G. Lammertink, Geometrical influence on mixing in helical porous membrane microcontactors, *J. Membr. Sci.* **378**, 351 (2011).
- [51] A. Groisman and V. Steinberg, Efficient mixing at low Reynolds numbers using polymer additives, *Nature* **410**, 905 (2001).
- [52] C. C. Hong, J. W. Choi, and C. H. Ahn, A novel in-plane passive microfluidic mixer with modified Tesla structures, *Lab Chip* **4**, 109 (2004).
- [53] T. Burghelea, E. Segre, and V. Steinberg, Mixing by Polymers: Experimental Test of Decay Regime of Mixing, *Phys. Rev. Lett.* **92**, 164501 (2004).

- [54] T. Krishnaveni, T. Renganathan, J. R. Picardo, and S. Pushpavanam, Numerical study of enhanced mixing in pressure-driven flows in microchannels using a spatially periodic electric field, *Phys. Rev. E* **96**, 033117 (2017).
- [55] H. Chen and J. C. Meiners, Topologic mixing on a microfluidic chip, *Appl. Phys. Lett.* **84**, 2193 (2004).
- [56] Y. Yu, L. Shang, G. Gao, Z. Zhao, H. Wang, and Y. Zhao, Microfluidic lithography of bioinspired helical micromotors, *Angew. Chem.* **129**, 12295 (2017).
- [57] Y. Kim, B. Kuczynski, P. R. LeDuc, and W. C. Messner, Modulation of fluidic resistance and capacitance for long-term, high-speed feedback control of a microfluidic interface, *Lab Chip* **9**, 2603 (2009).
- [58] E. Villermaux, A. D. Stroock, and H. A. Stone, Bridging kinematics and concentration content in a chaotic micromixer, *Phys. Rev. E* **77**, 015301 (2008).
- [59] R. D. Sawyers, M. Sen, and H. C. Chang, Effect of chaotic interfacial stretching on bimolecular chemical reaction in helical-coil reactors, *Chem. Eng. J.* **64**, 129 (1996).
- [60] X. Niu and Y. K. Lee, Efficient spatial-temporal chaotic mixing in microchannels, *J. Micromech. Microeng.* **13**, 454 (2003).